

Effects of catalyst:Ba molar ratio on the structure and luminescence properties of BaCO₃:1% Eu³⁺, 2% Dy³⁺ phosphors synthesized using sol-gel process.

AS Tebele*, SV Motloun and FB Dejene

Department of Physics, University of the Free State (Qwaqwa Campus), Private Bag X13, Phuthaditjhaba, 9866, South Africa

*Corresponding author.e-mail address: tebeleas@qwa.ufs.ac.za

Abstract. BaCO₃:1% Eu³⁺, 2% Dy³⁺ powders were synthesized by sol-gel process at a relatively low temperature ~ 80 0C. Metal nitrates were used as the source of metal ions and citric acid as a chelating agent. The catalyst:Ba molar ratio in the solution were varied from 1.0 - 2.5 during synthesis. The annealed powder samples were characterized by X-ray diffraction (XRD), scanning electron microscopy (SEM) and photoluminescence (PL) spectroscopy. The XRD data revealed that the annealed samples consist of orthorhombic BaCO₃ with extra peaks of BaO impurities at the lower catalyst content. Morphology of the phosphor was influence by the catalyst:Ba molar ratio. PL spectra indicated that the emission peaks appears at different wavelength positions 376, 531, 589 and 616 nm with the most intense peak at 616 nm. The emission at 376 nm is attributed to the changes in crystal field surrounding the activators. Emission peak at 531 nm is attributed to the host emission due to defects, while the emission peak at 589 nm is assigned to magnetic dipole ⁵D₀-⁷F₁ transitions in Eu³⁺ ion. The emission peak at 616 nm is attributed to hypersensitively force electric dipole ⁵D₀-⁷F₂ transitions in Eu³⁺ ion.

Keywords: Luminescence; BaCO₃:1% Eu²⁺, 2% Dy³⁺; catalyst:Ba; Sol-gel

1. Introduction

Metal carbonates are abundant minerals in nature and are of important interest in material research due to their promising applications such as optical materials, effective catalyst, separation technology, drug-delivery and pigment [1-5]. Barium carbonate (BaCO₃) also known as witherite is one of the well-known metal carbonates used in magnetic materials, television kinescope Glass-Shell and water cleaning [6]. Metal carbonates have shown to be good host lattice for various dopants or foreign atoms. Introduction of foreign atoms into the host lattice is known to affect the luminescence properties of the material [7-10]. It is well known rare earth ions have been playing an important role in modern lighting and display field due to abundant emission colors based on their transitions [11]. Furthermore, BaCO₃ is expected to show excellent luminescence properties by doping with rare-earth ions [12]. Eu³⁺ doped CaCO₃ phosphor with red emission prepared by microwave synthesis has been reported by Kang et al. [13]. Their results [13] shows that the red luminescence can be attributed to the transitions from the ⁵D₀ excited level to the ⁷F_{J=0,4} levels of Eu³⁺ ions with the mainly electric dipole transition ⁵D₀ → ⁷F₂ (614 and 620 nm). SrCO₃:Eu³⁺ microneedles through a large-scale and facile hydrothermal method without any template and further annealing treatment have been reported by Yang et al. [14]. In their results [14] they found a strong red

emission corresponding to the ${}^5D_0 \rightarrow {}^7F_{J=1-4}$ transitions of Eu^{3+} ions. The luminescent properties of $\text{CaCO}_3:\text{Eu}^{3+}$, $\text{BaCO}_3:\text{Eu}^{3+}$ and $\text{SrCO}_3:\text{Eu}^{3+}$ prepared by simple and convenient synthetic route containing H_2O and EG (ethylene glycol) with various compositions has been reported by Shi et al. [15]. Furthermore, their results [15] show three red emission spectra which seems to be equal in shape except for the intensity differences between them. Therefore, it is expected that $\text{BaCO}_3:\text{Eu}^{3+}, \text{Dy}^{3+}$ can be used as an FED (Field Emission Display) phosphor for practical application. So it is very important to synthesize $\text{BaCO}_3:\text{Eu}^{3+}, \text{Dy}^{3+}$ and understand the luminescent mechanism. BaCO_3 crystallizes in the orthorhombic system [16]; hence, there is continued interest in synthesizing of BaCO_3 with controlled morphologies [17]. Sreedhar et al. [24] report the synthesis and characterization of BaCO_3 nanocrystallite using natural polymer, gum acacia and they obtain pure orthorhombic structure in XRD analysis. Wang et al. [6] report a new route to the synthesis of BaCO_3 crystals by the induction of bacillus pasteurri and they found sphere-like and rod-like morphology with a diameter of 7 and 1 μm , respectively. At present, numerous methods have been reported on the preparation of BaCO_3 nanostructures including precipitation-electrodeposition reaction [19], reversed micelle method [20], polyvinylpyrrolidone-assisted method [21], high-gravity method [22] and sol-gel method [23]. The sol-gel technique offers the advantages such as excellent control over the stoichiometry, homogeneous particle distribution, good reactivity between components, nano-size particles and allows lower processing temperature [16]. In this work, the effect of varying the catalyst:Ba molar ratio in $\text{BaCO}_3:1\% \text{Eu}^{3+}, 2\% \text{Dy}^{3+}$ nanophosphor synthesized by the sol-gel technique is investigated. The main aim is to develop red light emitting phosphor for applications in pigment.

2. Experimental

The powders of $\text{BaCO}_3:1\% \text{Eu}^{3+}, 2\% \text{Dy}^{3+}$ phosphors with different catalyst:Ba molar ratio ranging from 1.0 – 2.0 were prepared by sol-gel process. Note that the Ba concentration was kept constant at 1 mol. The nitrates; $\text{Ba}(\text{NO}_3)_2$ (99%), $\text{Al}(\text{NO}_3)_3 \cdot 9\text{H}_2\text{O}$ (98.5%), $\text{Eu}(\text{NO}_3)_3 \cdot 5\text{H}_2\text{O}$ (99.9%), $\text{Dy}(\text{NO}_3)_3 \cdot 5\text{H}_2\text{O}$ (99%) were used as the starting materials and $\text{C}_6\text{H}_8\text{O}_7 \cdot \text{H}_2\text{O}$ (citric acid) (99%) was used as a catalyst. These nitrates and the catalyst were dissolved in deionized water and stirred constantly on magnetic stirrer at a temperature $\sim 80^\circ\text{C}$ until gelation. The prepared white gels were dried at 130°C in an oven for 4 hour. The dried gel was ground and subsequently annealed at 800°C for 2 hours. The crystal structure of the samples was characterized by powder X-ray diffraction (Bruker AXS Discover diffractometer) with $\text{CuK}\alpha$ (1.5418\AA) radiation. The surface morphology of the phosphor powder was established using a Shimadzu Superscan ZU SSX-550 electron microscope (SEM). PL excitation and emission spectra were obtained by using Xenon lamp (Hitach F-7000 fluorescence spectrophotometer).

3. Results and discussion

3.1. Structure

For all samples the (111) diffraction peak were deconvoluted as shown in figure 1 (a) to distinguish between (111) and (102). The average d-spacing for the (111) peak was estimated to be 12.165\AA and the lattice parameters were calculated to be $a = 6.415\text{\AA}$, $b = 5.302\text{\AA}$ and $c = 8.870\text{\AA}$, which are very close to those of JCPDS card no. 45-1471 where $d = 12.202\text{\AA}$, and the lattice parameters are $a = 6.433$, $b = 5.314$ and $c = 8.903\text{\AA}$ [24]. Figure 1 (b) and (c) shows the diffractions patterns of the annealed $\text{BaCO}_3:1\% \text{Eu}^{3+}, 2\% \text{Dy}^{3+}$ powders for the co-doped and un-doped 1.0 catalyst:Ba molar ratio and for co-doped samples at varying catalyst:Ba molar ratios, respectively. The XRD patterns of all prepared samples matches with the peaks of BaCO_3 JCPDS card no. 45-1471. However, the XRD detected an impurity (shown by asterisk (*) in figure 1 (b) and (c)), which can be attributed to the BaO [25]. If the catalyst content is too much as shown in figure 1 (c) (e.g. 2.5 molar ratio), the results reveal that there are no BaO impurity which suggest the single phase formation at the higher molar ratio. Furthermore, the single phase formation at higher molar ratio also suggests that the foreign atoms (e.g. Eu^{3+} and Dy^{3+}) were fully incorporated into the host matrix [26]. Therefore, catalyst:Ba molar ratio at 2.5 does not affect the crystal structure of the phosphor, which implies that catalyst at this stage helps BaCO_3 to fully incorporate with these foreign atoms (Eu^{3+} and Dy^{3+}). From Feilong et al. report [25], it is known that $\text{Ba}(\text{NO}_3)_2$ does not easily dissolve

in deionized water, and therefore, from this results we infer that more catalyst content might be necessary to fully catalyse the dissolving of $\text{Ba}(\text{NO}_3)_2$ in deionized water. Thus, this might serve as a good reason why the single phase structure is obtained at higher mole fraction as shown in figure 1 (c). The grain sizes of the powders with various Catalyst:Ba molar ratio for 1.0 (un-doped), 1.0 (co-doped), 1.3, 1.5, 1.8 and 2.5 were estimated from the main diffraction peak (111) by using the Scherrer formula [27] and they were found to be 85, 82, 84, 85, 69 and 70 nm, respectively. It is therefore, concluded that varying catalyst:Ba molar ratio influences the crystallites. Figure 1 (d) shows the analysis of the most intense peak (111). As it can be seen that there is slight shift to the higher diffraction angle in the (111) peak as the catalyst:Ba molar ratio is varied, and that is attributed to the change in the lattice spacing [26]. Shifting to the higher angle is also attributed to the decrease in d-spacing as the foreign atoms are incorporated into the BaCO_3 matrix [26] as shown in figure 1 (e). This is due to the substitution of bigger atom Ba^{2+} (atomic radius 1.61 Å) [27] with smaller atoms Eu^{3+} (0.95 Å) [28] and Dy^{3+} (1.08 Å) [29]. It is therefore, proposed that the catalyst:Ba molar ratio influences the d-spacing. The d-spacing as a function of catalyst:Ba molar ratio shows the parabolic behaviour as depicted in figure 1 (e) for the (111) diffraction peak. The decrease in d-spacing is due to the increase in catalyst:Ba molar ratio, that is, due to the substitution of Ba^{2+} with Eu^{3+} and Dy^{3+} as mentioned above. Thus, the mole ratio is facilitating the substitutions or knocking-off the atoms in the host matrix. However, as the catalyst:Ba molar ratio is increased further, the decrease in d-spacing reaches a critical point at 1.9 (catalyst:Ba) molar ratio and then increases. Similar behaviour to our results has been observed by Motloug et al. [26] and the ref therein.

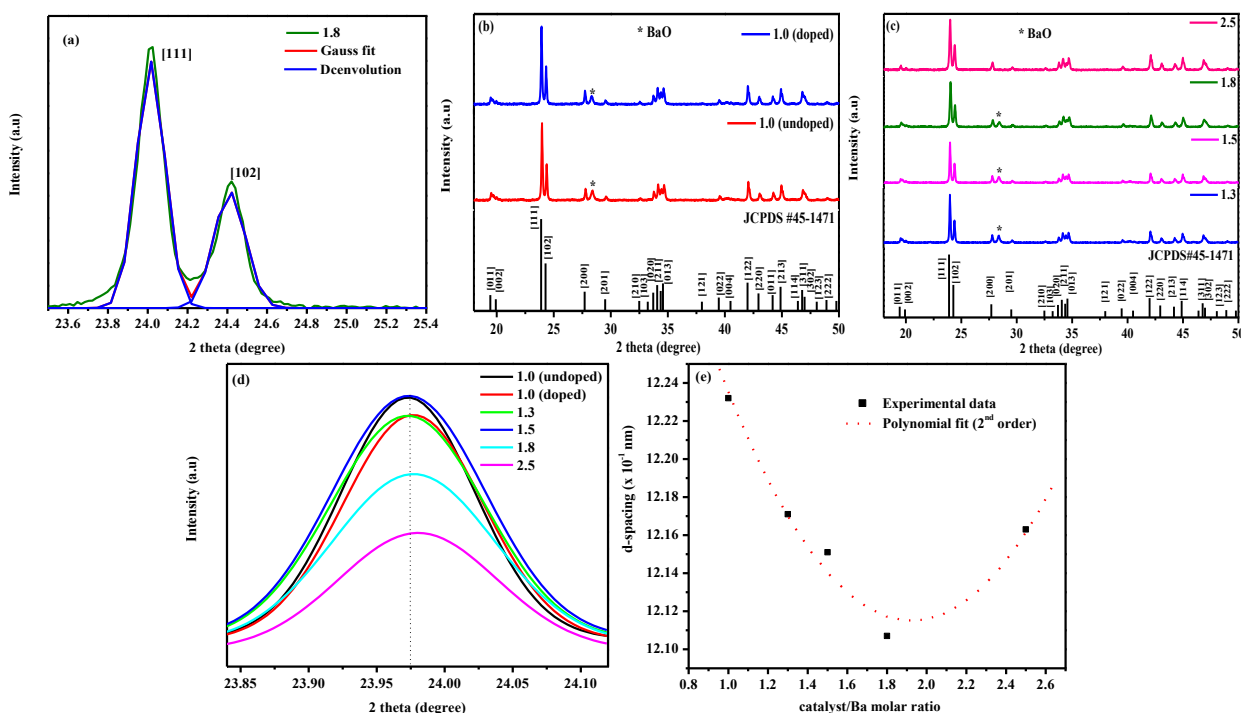


Figure 1 (a) Deconvolution of 1.8 catalyst:Ba molar ratio X-ray patterns of the (b) 1.0 (co-doped) and 1.0 (un-doped) (c) BaCO_3 :1% Eu^{3+} , 2% Dy^{3+} at varying catalyst:Ba molar ratio (d) Analysis of (111) Peak (e) d-spacing as a function of catalyst:Ba molar ratio.

3.2. Phosphor morphology

The surface morphologies of the annealed samples were observed by SEM micrographs shown in figure 2 (a) – (f). Fig. 2 (a) shows the dispersal of small irregular particles at 1.0 (catalyst:Ba) molar ratio for the

un-doped BaCO_3 which consists of voids morphology. At 1.0 molar ratio for the co-doped BaCO_3 the micrograph shows the dispersal of small irregular particles on the surface of the large agglomerated particle (see figure 2 (b)), which is similar to figure 2 (c) – (f). It is interesting to observe that as the catalyst:Ba molar ratio is increased to 2.5, as shown in figure 2 (f), the particles become more agglomerated with the porous morphology on the surface. These results showed that varying catalyst:Ba molar ratio does not affect morphology of the phosphor which agrees with XRD analysis. It is suggested that porous/voids are formed by degassing during annealing process [30], that is, pores originate from gas entrapment due to improper adhesion at certain places [31].

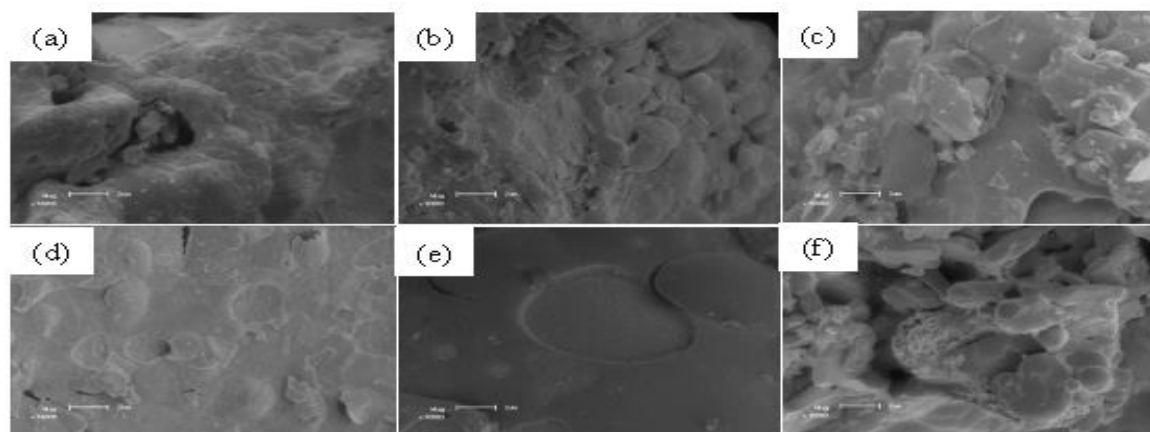


Figure 2 SEM images of the $\text{BaCO}_3:1\% \text{Eu}^{3+}, 2\% \text{Dy}^{3+}$ for various catalyst:Ba molar ratio for (a) 1.0 (un-doped), (b) 1.0 (co-doped), (c) 1.3, (d) 1.5, (e) 1.8 and (f) 2.5.

3.3 Photoluminescence characteristics

Excitation photoluminescence spectra of the $\text{BaCO}_3:1\% \text{Eu}^{3+}, 2\% \text{Dy}^{3+}$ are shown in figure 3 (a). It was observed that the main peaks are at 260 and 303 nm. The absorption band with maximum at 260 nm is attributed to the charge transfer (CT) state of $\text{Eu}^{3+} - \text{O}^{2-}$ [32]. The absorption at 303 nm corresponds to the host absorption [33]. The emission spectra of the $\text{BaCO}_3:1\% \text{Eu}^{3+}, 2\% \text{Dy}^{3+}$ powders are shown in figure 3 (b). The PL emission reveals that un-doped powder has peaks at 400 and 531 nm. These emission peaks are therefore attributed to originate from the host material. Both emission bands are assumed to be due to the band-to-band and defects level in the host. The co-doped powders have the emission peaks at different positions 376, 531, 589 and 616 nm with the most intense peak at 616 nm. The emission at 376 nm is attributed to the changes in crystal field surrounding the activators [34]. It can be seen that the emission peak at 531 nm arises from the un-doped 1.0 (catalyst:Ba) molar ratio and therefore is attributed to the defects emission in the host material (as mentioned above). The emission peak at 589 nm is assigned to magnetic dipole transitions ${}^5\text{D}_0-{}^7\text{F}_1$ of Eu^{3+} [35]. The emission peak at 616 nm is attributed to hypersensitively force electric dipole transitions ${}^5\text{D}_0-{}^7\text{F}_2$ of Eu^{3+} [35]. Figure 3 (c) shows the deconvolution of 2.5 (catalyst:Ba) molar ratio as the same as in figure 3 (b) when excited at the same excitation energy and it shows that there are two emission peaks at 350 and 376 nm. The emission peak at 350 nm is attributed to ${}^6\text{H}_{15/2}-{}^4\text{M}_{15/2}, {}^6\text{P}_{7/2}$ from Dy^{3+} ions [33] and 376 nm is attributed as mentioned above. This emission spectra show some changes in peak shape, especially at high energy (<400 nm) [33]. This behavior is observed at the higher molar ratio (e.g. 1.8 and 2.5) and it is assigned to changes in crystal field surrounding the activators [34], which agrees very well with the XRD findings. Moreover, this PL results clearly shows that varying catalyst:Ba molar ratio changes the dopants environment in the

host material. Thus, the variation of catalyst:Ba molar ratio affected the luminescent properties of $\text{BaCO}_3:1\% \text{Eu}^{3+}, 2\% \text{Dy}^{3+}$ phosphors.

Figure 3 (d) shows the afterglow curve of $\text{BaCO}_3:1\% \text{Eu}^{3+}, 2\% \text{Dy}^{3+}$ phosphor at room temperature after exciting by 260 nm when monitoring the red emission at 616 nm. The decay characteristics of this phosphor indicates that the shape of afterglow decay curves of the samples at the varying catalyst:Ba molar ratio are similar, which indicates that all the samples have the same afterglow decay mechanism. The afterglow intensity gradually becomes zero after 2750 ms. Therefore, when the excitation source is switched off, the relaxation of these secondary ions from deep traps is very slow; this leads to the long persistence of phosphor [18]. When the mole fraction is 1.5 it demonstrate a significant improvement in initial luminescent brightness and long afterglow. The results are consistency with the measurements of PL emission in figure 3 (b), where 1.5 catalyst:Ba molar ratio is observed with the highest emission intensity.

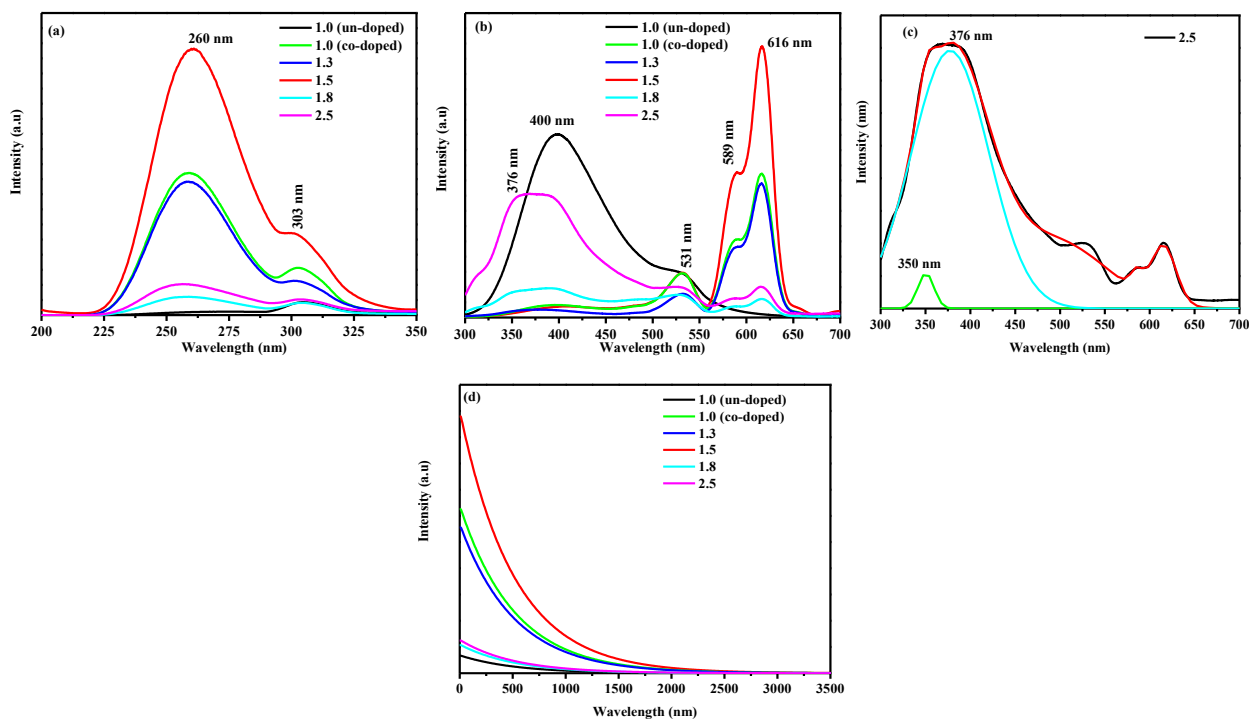


Figure 3 PL spectra of the annealed $\text{BaCO}_3:1\% \text{Eu}^{3+}, 2\% \text{Dy}^{3+}$ (a) excitation spectra ($\lambda_{\text{em}} = 616 \text{ nm}$) (b) emission spectra ($\lambda_{\text{ex}} = 260 \text{ nm}$) (c) 2.5 molar ratio deconvolution (d) Afterglow decay curve ($\lambda_{\text{ex}} = 260 \text{ nm}$).

4. Conclusion

$\text{BaCO}_3:1\% \text{Eu}^{3+}, 2\% \text{Dy}^{3+}$ phosphors powders were successfully synthesized using sol-gel process. XRD results show that when the powders are annealed at 800°C , the crystalline structure shows orthorhombic BaCO_3 with some impurities such as BaO. If the catalyst content is too much, the foreign atoms (e.g. Eu^{3+} and Dy^{3+}) distribute homogeneously in the host material to form pure orthorhombic structure. SEM images showed irregular particles morphology. The excitation peaks were found to be 260 and 303 nm, which are attributed to the charge transfer (CT) state of $\text{Eu}^{3+} - \text{O}^{2-}$ and the host absorption. The most intense emission peak at 616 nm is assigned to hypersensitively force electric dipole transitions ${}^5\text{D}_0 - {}^7\text{F}_2$ transitions of Eu^{3+} . The amount of citric acid affected the luminescent properties of $\text{BaCO}_3:1\% \text{Eu}^{3+}, 2\% \text{Dy}^{3+}$ phosphors. The decay curve show that all samples have the same afterglow behaviour and it also shows the improvement in initial luminescent brightness and long afterglow.

Reference

- [1] Jacob D S, Joseph A, Mallenahalli S P, Shanmugam S, Makhluf S, Calderon-Moreno J, Koltypin Y, Gedanken A 2005 *Angew Chem Int Ed* **44** 6560–6563.
- [2] Ma H C, Bai X T, Zheng L Q 2011 *CrystEngComm* **13** 3788–3793.
- [3] Wei W, Ma G H, Hu G, Di Y, Mcleish T, Su Z G, Shen Z Y 2008 *J. Am. Chem. Soc* **130** 15808–15810.
- [4] Macketta J J. 1977 *Encyclopedia of Chemicals Processing and Design* (Marcel Dekker: New York).
- [5] Dalas E, Klepetsanis P, Koutsoukos P G 1999 *Langmuir* **15** 8322.
- [6] Wang L N, Huo J C, Liu S X, Lei Y L 2011 *Chinese. J. Struct. Chem* **30** 738-742.
- [7] Ci Z, Wang Y 2009, *J. Electrochem. Soc.* **156** J267-J272.
- [8] Li P L, Wang Z J, Yang Z P, Guo Q L 2011 *Chin. Phys. Lett.* **1** 017801.
- [9] Chen R, Wang Y, Hu Y, Hu Z, Liu C 2008 *J. Lumin.* **128** 1180-1184.
- [10] Hwang K S, Kang B A, Kim S D, Hwangbo S, Kim J T 2011 *Bull. Mater. Sci* **34** 10591062.
- [11] Xue Y, Ren X, Yu M 2012 *solid state sciences* **14** 1086-1091.
- [12] Ci Z, Wang Y 2009, *J. Electrochem. Soc.* **156** J267-J272.
- [13] Kang M, Liu J, Yin G and Sun R 2009 rare metals **28** 439-444.
- [14] Yang J, Liu X, Li C Quan Z, Kang D and Lin J 2007 *J. Crystal Growth* **303** 480-486.
- [15] Bao SP, Chen XY, Li Z, Yang BJ and Wu Y C 2010 *CrystEngComm* **13** 2511-2520.
- [16] Zelati A, Amirabadizadeh A, Kompany A 2011 *IJCEA* **02**.
- [17] Sumy J, Sarala U, Kamathi V P 2009 *J. Chem. Sci.* **121** 685–691.
- [18] Sreedhar B, Vani C S, Devi D K, Rao M V B, Rambabu C 2012 *J. Mat. Sci.* **2** 5-13.
- [19] Bei C, Xiaoxiao Y, Jiagu Y, Xiujian Z 2006 *Rare Metals* **25** 382.
- [20] Karagiozov C, Momchilova D 2005 *Chem. Eng. Process.* **44** 115.
- [21] Lv S, Li P, Sheng J, Sun W 2007 *Mat. Lett.* **61** 4250.
- [22] Chen L, Shen Y, Xie A, Zhu J, Wu Z, Yang L 2007 *Cryst. Res. Technol.* **42** 886.
- [23] Clifford Y T, Chia-te T, Hwai-shen L 2006 *Chem. Eng. Sci.* **61** 7479.
- [24] Zelati A, Amirabadizadeh A, Kompany A, Larimi Z M 2011 *ICCCP* **10** 146-150.
- [25] Feilong S. Junwu Z 2011 *Journal of rare earth* **29** 326-329.
- [26] Motloun S V, Dejene B F, Swart H, Ntwaeaborwa O M 2014 *J. Sol-gel Sci. technol.* **70** 422-427.
- [27] Ohta R, Onda Y, Kojima S 2011 *J Korean phys.soc.* **59** 2471-2474.
- [28] Cheng B, Qu S, Zhou H, Wang Z 2006 *Nanoteq.* **17** 2982-2987.
- [29] Li Y, Chang Y, Lin Y, Chang Y, Lin Y 2007 *J. alloys compd.* **439** 367-375.
- [30] Granados-Correa F, Jimenez-Reyes M 2011 *Sep. Sci. Technol.* **46** 2360–2366.
- [31] Wang Z, Kulkani A, Deshpande S, Nakamura T, Herman H 2003 *Acta Mater.* **51** 5319-5334.
- [32] Ohta R, Onda Y, Kojima S 2011 *J Korean phys.soc.* **59** 2471-2474.
- [33] Li Y, Chang Y, Lin Y, Chang Y, Lin Y 2007 *J. alloys compd.* **439** 367-375.
- [34] Zhou L, Choy W C H, Shi J., Gong M, Liang H 2006, *Mat. Chem. Phys.* **100** 372-347.
- [35] Ntwaeaborwa O M, Nsimama P. D, Pitale S, Nagpure I M, Kumar V, Coetsee E, Terblans J J, Swart H C, Sechogela P T 2010 *J. Vac. Sci. Technol. A* **28**.